Magnetic Resonance Materials in Physics, Biology and Medicine
https://doi.org/10.1007/s10334-024-01185-4

RESEARCH ARTICLE

Assessing biological self-organization patterns using statistical complexity characteristics: a tool for diffusion tensor imaging analysis

Antonio Carlos da S. Senra Filho[1] · **Luiz Otávio Murta Junior**[2] · **André Monteiro Paschoal**[1]

Received: 1 April 2024 / Revised: 24 June 2024 / Accepted: 28 June 2024

Abstract

Object Diffusion-weighted imaging (DWI) and diffusion tensor imaging (DTI) are well-known and powerful imaging techniques for MRI. Although DTI evaluation has evolved continually in recent years, there are still struggles regarding quantitative measurements that can benefit brain areas that are consistently difficult to measure via diffusion-based methods, e.g., gray matter (GM). The present study proposes a new image processing technique based on diffusion distribution evaluation of López-Ruiz, Mancini and Calbet (LMC) complexity called diffusion complexity (DC).

Materials and Methods The OASIS-3 and TractoInferno open-science databases for healthy individuals were used, and all the codes are provided as open-source materials.

Results The DC map showed relevant signal characterization in brain tissues and structures, achieving contrast-to-noise ratio (CNR) gains of approximately 39% and 93%, respectively, compared to those of the FA and ADC maps.

Discussion In the special case of GM tissue, the DC map obtains its maximum signal level, showing the possibility of studying cortical and subcortical structures challenging for classical DTI quantitative formalism. The ability to apply the DC technique, which requires the same imaging acquisition for DTI and its potential to provide complementary information to study the brain's GM structures, can be a rich source of information for further neuroscience research and clinical practice.

Keywords Diffusion tensor imaging · Statistical complexity · MRI · Brain

Introduction

Diffusion-weighted imaging (DWI) and diffusion tensor imaging (DTI) are well-known and powerful MR imaging techniques. After its first presentation in the mid-1980s [1], diffusion-based imaging techniques have undergone more than three decades of development and application. The ability to infer quantitative diffusion measurements in the biological environment has been one of the most important features of diffusion-weighted images [2–5]. Considering the most common approach using the tensorial representation for DTI images [6], several diffusion-based representations can be achieved, including common measurements, such as the fractional anisotropy (FA) and apparent diffusion coefficient (ADC). These forms of diffusion characterization have been widely useful for studying the human body in a non-invasive way [7–9].

However, the limitations of the FA and ADC formalism in some studies, particularly for human brain evaluation, are well-known. The low tissue contrast for apparent diffusion coefficient (ADC) maps and the measurement variation present in crossing-fiber orientations for FA maps are some examples of the challenges that are continually studied in the scientific community [4, 6, 8]. Several ideas have been proposed over the years to create novel image-processing techniques to provide complementary information for usual FA and ADC measurements. For this purpose, the application of physical statistics formalism has made contributions to DTI evaluation, e.g., by considering Shannon's information theory [10–14].

Although the contribution of physical statistics formalism has led to advances in DTI evaluation, there are still struggles regarding quantitative measurements that can benefit brain areas that are consistently difficult to measure via diffusion-based methods, e.g., gray matter (GM) [15,

✉ Antonio Carlos da S. Senra Filho
acsenrafilho@alumni.usp.br

[1] Department of Cosmic Rays and Chronology, University of Campinas, São Paulo, Brazil

[2] Department of Computing and Mathematics, University of Sao Paulo, São Paulo, Brazil

Published online: 28 July 2024

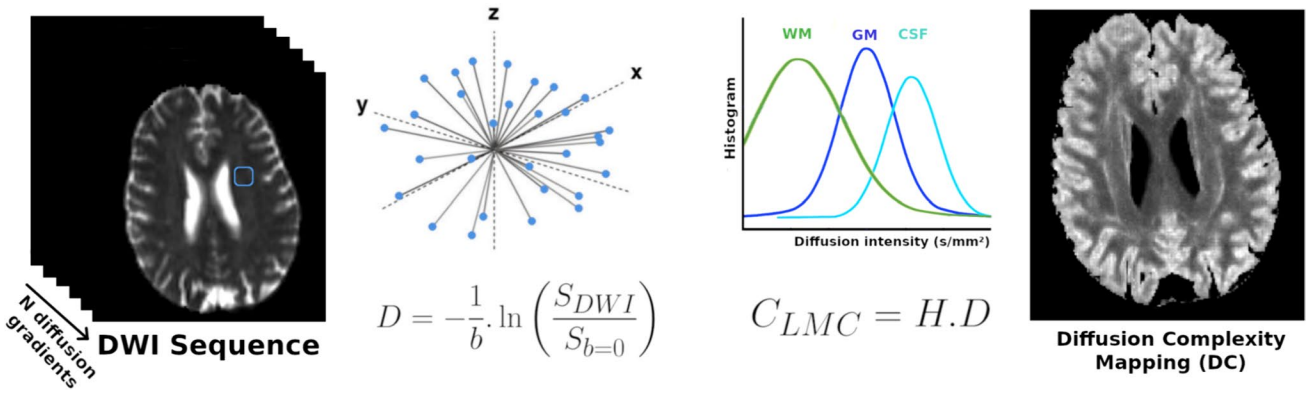

Fig. 1 Schematic diagram illustrating the Diffusion Complexity (DC) calculation. The raw diffusion-weighted diffusion (DWI) sequence is used as the source of information for determining diffusion signal distributions, and the probability diffusion distribution obtained from the diffusion signal histogram can be applied to the LMC complexity formulation as expressed in Eq. (1). It is expected that the differences in the microenvironment of each brain tissue can provide a different response in the diffusion complexity measure as seen schematically in the colored histogram distribution patterns (e.g., White Matter in green, Gray Matter in blue and CSF in light blue)

16]. We propose a novel image processing technique based on diffusion space analysis and the López-Ruiz, Mancini, and Calbet (LMC) complexity measure [17, 18], which we denote as diffusion complexity (DC) mapping.

This study explains the DC formalism and presents its calculation and computational algorithm. The definition of DC mapping followed that in the manuscript. The experimental design focused on evaluating the healthy human brain using a DTI imaging protocol and, finally, a comprehensive analysis showing the potential of this novel image processing technique and its contribution to the diffusion imaging modality in MRI.

Materials and methods

Diffusion complexity measurement

The first concept adopted in measuring diffusion complexity is given by the definition of the signal distribution that is analyzed. In DWI, the acquired signal is a direct measure of water self-diffusion in biological tissue [3, 19]. Therefore, we assume that the signal distribution is the diffusion magnitude obtained from the diffusion image. Recall that we are not considering the tensor representation, which is usually adopted for FA and ADC measurements. Instead, we collect the voxelwise diffusion orientation, given by the N diffusion gradients and the b-value reference; therefore, we account for the histogram of the diffusion signal. In other words, the normalized histogram is used to represent the probability density function for the diffusion magnitude observed in each voxel and then being able to apply the LMC calculation given in Eq. (1). The diagram illustrated in Fig. 1 shows the signal distribution construction for the DC mapping.

$$C_{LMC} = H.D = -\left(k\sum_{i=1}^{N} p_i \cdot \log p_i\right).\left(\sum_{i=1}^{N}\left(P_i - 1/N\right)^2\right) \quad (1)$$

where H is Shannon's entropy, D is the disequilibrium estimate [17], and N represents the total diffusion gradients used in DTI image acquisition.

Database

All the DTI images used in this study were collected from public open-source databases. The main selection criteria for the imaging database were based on the availability and reproducibility of the data for further evaluation. Another important criterion was that the MRI-DTI images were comparable to those of routine clinical practice. The databases Open Access Series of Imaging Studies (OASIS-3)[1] [20] and TractoInferno[2] [21] were used.

The general image acquisition protocol for both databases is described as follows: (i) T1-weighted (T1-w) images using the accelerated sagittal 3D IR-SPGR protocol, slice thickness of 1.5 mm, TR ranging from 7.3 to 9.7 ms, TE ranging from 3.0 to 4.0 ms, TI ranging from 20 to 400 ms, flip angle of 11°, matrix size of $256 \times 256 \times 128$ and in-plane axial isotropic resolution of 1.0 mm^2; (ii) DTI images using the EPI protocol, TR ranging from 1800 to 9200 ms, TE ranging from 70 to 93 ms, angle = 90°, SENSE reduction factor ranging from 2.5, gradient directions of 21–64 orientations of b1 values ranging from 700 to 1000 s/mm^2 and single b = 0 s/mm^2 were also acquired alongside the DWI images and 1.75–2.3 mm^3 isotropic voxels. The MRI scanners used

[1] https://sites.wustl.edu/oasisbrains/.

[2] https://openneuro.org/datasets/ds003900/versions/1.1.1.

were 3 T Philips Achieva, 3 T Siemens Prisma, 3 T Siemens Trio, 3 T Siemens Magnetom TIM Trio, and 3 T GE Discovery MR750. More details are explained in each database citation, i.e., OASIS-3 [20] and TractoInferno [21].

Due to the interest in evaluating our DC mapping method, only a subset of the healthy individuals comprising our image dataset was adopted. Therefore, anatomical changes related to brain diseases or natural brain aging were not considered. Thus, the following image databases were used in this study: (i) OASIS-3: 53 subjects ranging in age from 42 to 48 years, with a balance of 55%/45% right-handed male/female; (ii) TractoInferno: 62 subjects ranging in age from 38 to 45 years, 50%/50% right-handed male/female.

All the DTI image sequences were evaluated on standard quality control procedures [22, 23] to create a uniform database for quantitative analysis and follow the general DTI processing techniques debated by the scientific community. No additional image processing algorithms were applied to the DTI images to preserve the image quality as close as possible to the initial conditions.

Experiments

DTI quantitative analysis

The DTI images were obtained as raw DWI sequences in Nifti image format. First, the most common DTI quantitative maps were adopted, i.e., fractional anisotropy (FA) and apparent diffusion coefficient (ADC). DTI map reconstruction was performed using FMRib's Diffusion Toolbox (FDT), FMRIB Software Library, FMRIB, Oxford, UK [24, 25], with the standard configuration and tensor diffusion representation. The DC map was calculated using the raw DWI sequences, as shown in Fig. 1 and Eq. 1. All three DTI maps were obtained, maintaining the same original image space and image metadata. For the DC map, we used an in-house implementation (see Sects. "Material and methods", Diffusion complexity measurement", "Database" "Results").

Regarding the brain tissue analysis, we used the T1-w images for both brain tissue segmentation and spatial normalization with the brain atlas. Once the T1-w image of the subject has been prepared, image registration is performed to align the T1-w-based labels to the DTI image space. We adopted a 3D rigid operation for intrasubject normalization, and for brain atlas normalization, we used sequential 3D rigid, affine, and β-spline deformation [26]. In all these image spatial transformations, we adopted the ANTs image normalization toolkit [27]. We used the MNI-152 2 mm^3 resolution brain atlas, defined by the Harvard–Oxford with subcortical brain tissue parcellation [28, 29], assuming that the brain tissue segmentation was restricted to at least 25% of the tissue probability [30].

Signal intensity and contrast-to-noise evaluation

This signal intensity evaluation was conducted by comparing the major brain tissues, i.e., gray matter (GM), white matter (WM), and cerebrospinal fluid (CSF). Additional brain image structures were also analyzed, focusing on subcortical brain structures, i.e., the thalamus, caudate, putamen, pallidum, hippocampus, amygdala, and accumbens [28, 29].

The contrast-to-noise ratio was evaluated assuming a direct calculation of the brain tissue of interest over a standard brain tissue as defined in Eq. (2).

$$CNR_{\|A-B\|} = \frac{|S_A - S_B|}{\sigma_b} \tag{2}$$

where the region of interest adopted for the noise estimate, σ_b, is the CSF signal in intraventricular spaces, i.e., σ_{CSF}.

Tissue homogeneity evaluation

We adopted the coefficient of variation as the brain tissue homogeneity measurement. Therefore, it is interesting to identify whether the DTI quantitative map presents signal stability in anatomically homogenous regions. The coefficient of variation, CV_t, measured over a tissue region is given by Eq. (3).

$$CV_t = \frac{\sigma_t}{\mu_t} \tag{3}$$

where μ_t is the mean and σ_t is the standard deviation values for tissue t.

Code implementation and computation requirements

The DC mapping method was developed using the Insight Toolkit (ITK) open-source framework based on the C++ programming template. The ITK code is openly distributed on the GitHub repository[3] maintained by the CSIM laboratory.[4] In addition, a command-line plugin (documentation website[5]) was developed for 3DSlicer[6] software, which is another useful tool for medical image analysis. All these implementations were aimed at assisting the research and medical community in analyzing and using the DC map. Open imaging science promotes greater transparency, reproducibility, and collaboration

[3] https://github.com/CSIM-Toolkits/ITK.

[4] Computer in Signals and Images Laboratory, University of Sao Paulo, Brazil.

[5] https://www.slicer.org/wiki/Documentation/Nightly/Extensions/DiffusionComplexityMap.

[6] https://www.slicer.org/.

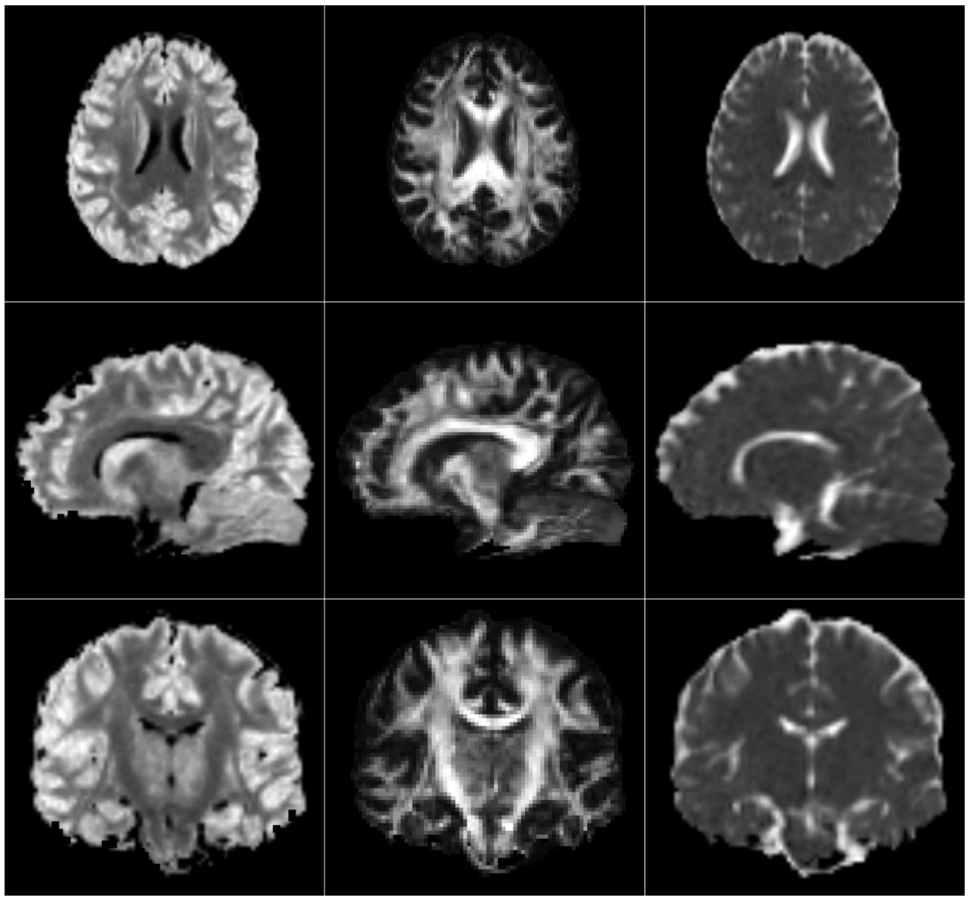

Fig. 2 Comparison of DC, FA, and ADC (columns) mapping for axial, sagittal and coronal orientations (rows). The DC map stands out for all three major brain tissues. In particular, the GM is significantly brighter in DCs as shown by FA and apparent diffusion coefficient (ADC) maps

in the imaging science field. The open-source 3D Slicer software can be customized and extended by the community, fostering innovation and continuous improvement by solving problems in imaging science.

All the computational experiments were performed using a computer with the following requirements: Linux OS, Mint 21.2 Cinnamon version 5.8.4, Intel i7-12700H core processor, 512 GB SSD, 16 GB 4.800 MHz DDR5 RAM and NVidia dedicated RTX 3060 GDDR6 6 GB GPU.

Results

A visual assessment was conducted at the initial examination to discern the basic signal configuration presented in the proposed method. As illustrated in Fig. 2, the global signal patterns for FA, ADC, and DC mapping can be compared. Initially, it was possible to distinguish the three primary brain tissues using DC, showing the WM, GM, and CSF. When assessed against the FA and ADC images, it is evident that there is a unique signal preference for WM and CSF, respectively; however, these conventional maps revealed low signal levels for the remaining brain tissues.

Figure 3 presents the quantitative signal levels, demonstrating a distinct separation between WM, GM, and CSF using a DC map. However, for FA and ADC signal evaluation, it is evident that WM and CSF tissues can be identified separately although the other tissues are not statistically distinguishable. For instance, considering the two-sample t-test hypothesis analysis with a significant p-value of 0.05, the FA maps for the GM-CSF comparison and the ADC maps for the WM-GM comparison showed no significant differences (p-value = 0.088 and p-value = 0.079, respectively). On the other hand, the DC map showed significant differences for all brain tissues, i.e., GM-WM (p-value $< 10^{-4}$), GM-CSF (p-value $< 10^{-4}$) and WM-CSF (p-value $< 10^{-4}$). As illustrated in Fig. 3, FA and ADC overlap in signal levels for GM/CSF and WM/GM, respectively. This observation was not observed in the DC image, which showed a distinctly separable signal distribution.

It is important not only to evaluate signal intensity but also to quantify the tissue contrast that can be achieved with each DTI map. The DC map is particularly noteworthy in providing relevant contrast for all major brain tissues, demonstrating significant differences among brain regions in the WM, GM, and CSF. As illustrated in Fig. 4, the CNR measurements revealed the level of tissue contrast achieved.

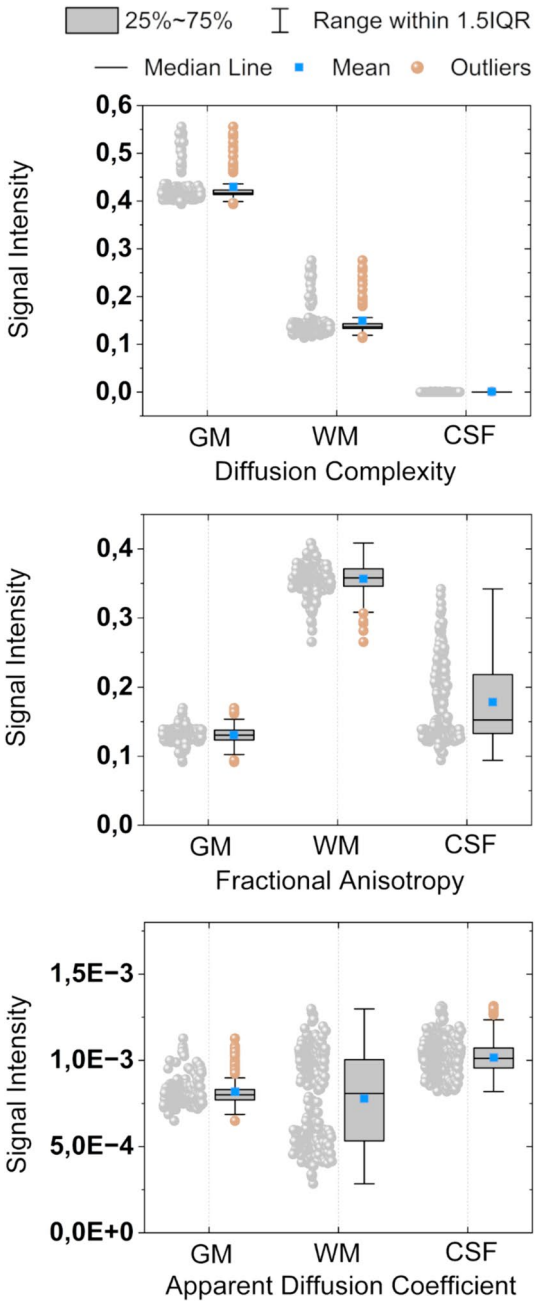

Fig. 3 Signal intensity evaluation for DC, FA, and ADC maps. The DC map presents a broad signal intensity for WM, GM, and CSF tissues in comparison to that of FA and ADC. Furthermore, all three brain tissues are well-separated in the DC map, which can be difficult to distinguish via FA (between the GM and CSF) and ADC (between the GM and WM)

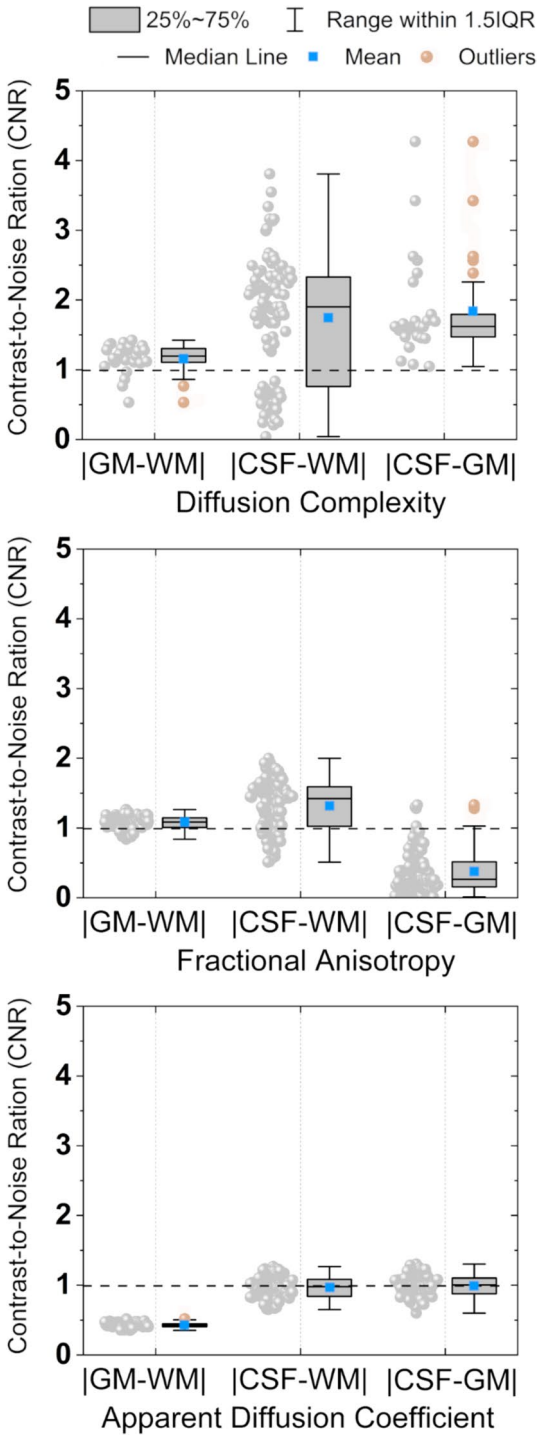

Fig. 4 Contrast-to-noise (CNR) evaluation for DC, FA, and ADC maps. The DC map retains a well-separated brain tissue contrast for all WM, GM, and CSF regions, revealing a strong signal intensity through image noise. On the other hand, FA and ADC maps struggle with signal differentiation among tissues with low contrast in these DTI maps, i.e., |CSF-GM| for FA and |GM-WM| for ADC

While the FA and ADC maps cannot provide reliable separation between some of these anatomical regions, the DC map shows greater CNR for all three major brain tissues and can be analyzed with a high level of confidence in the WM, GM, and CSF (details in Table 1). Furthermore, the average CNR for the DC map was approximately four times

Table 1 Summary of the relative average CNR gains obtained for DC compared to FA and ADC maps

	Average DC map CNR gain factor compared with			
	FA ($\mu \pm \sigma$ a.u.)	p-value	ADC ($\mu \pm \sigma$ mm^2/s)	p-value
$CNR_{\|GM\text{-}WM\|}$	1,21 ± 0,71	0,0011	1,85 ± 0,41	$< 10^{-4}$
$CNR_{\|CSF\text{-}WM\|}$	1,37 ± 0,22	$< 10^{-4}$	1,86 ± 0,56	$< 10^{-4}$
$CNR_{\|CSF\text{-}GM\|}$	3,82 ± 0,33	$< 10^{-4}$	1,83 ± 0,86	$< 10^{-4}$
$CNR_{\|WM\text{-}TAL\|}$	1,42 ± 0,34	$< 10^{-4}$	2,48 ± 0,81	$< 10^{-4}$
$CNR_{\|WM\text{-}CAU\|}$	1,98 ± 0,34	$< 10^{-4}$	2,43 ± 0,38	$< 10^{-4}$
$CNR_{\|WM\text{-}PUT\|}$	2,18 ± 0,33	$< 10^{-4}$	1,65 ± 0,89	$< 10^{-4}$
$CNR_{\|WM\text{-}PAL\|}$	1,17 ± 0,13	0,0595*	1,79 ± 0,08	$< 10^{-4}$
$CNR_{\|WM\text{-}HIP\|}$	1,29 ± 0,34	$< 10^{-4}$	1,31 ± 0,36	$< 10^{-4}$
$CNR_{\|WM\text{-}AMY\|}$	1,39 ± 0,45	$< 10^{-4}$	1,39 ± 0,22	$< 10^{-4}$
$CNR_{\|WM\text{-}ACC\|}$	1,67 ± 0,44	$< 10^{-4}$	1,76 ± 0,19	$< 10^{-4}$

The three permutation evaluations were considered for the major WM, GM, and CSF tissues. The subcortical brain regions are compared with their neighboring brain tissue, i.e., the WM

*p-values above the assumed significance level of 0.01

greater than that for the FA maps for the same tissues (see |CSF-GM| in Fig. 4). A similar pattern is observed for the ADC map, with the DC CNR showing an average increase of approximately 85% for all major brain tissue comparisons, i.e., $CNR_{|GM\text{-}WM|}$, $CNR_{|CSF\text{-}WM|}$ and $CNR_{|CSF\text{-}GM|}$. The CNR gains obtained for the major and subcortical brain areas are listed in Table 1.

In addition to the signal and CNR evaluation, it is essential to analyze the general tissue homogeneity obtained from each quantitative map. Figure 5 shows the global distribution of subcortical brain regions using DC, FA, and ADC maps. By comparing the global image patterns, it becomes clear that the DC map exhibits a more uniform spatial distribution within each region. Table 2 shows the CV results used to infer tissue homogeneity. The FA map displays significant variations in signal intensity within larger brain regions, while the ADC map maintains a consistent smoothness across varying brain areas.

Figure 6 contains additional information on tissue homogeneity, offering a more detailed examination of certain subcortical brain regions. Notably, the DC map exhibits variations in signal strength for closely related subcortical areas, such as Pallidum and Putamen. In contrast, the FA and ADC maps struggle to clearly represent the signals of those brain areas. While FA maps tend to show more fluctuations in the signal, the apparent diffusion coefficient (ADC) remains consistently smooth across all GM-related signals. Overall, the DC map can distinguish between GM structures and WM tissue, even in more subtle subcortical brain regions.

Discussion

DTI is a powerful tool for human brain analysis and has several applications in modern medicine. However, there are limitations concerning classical quantitative information, such as FA and apparent diffusion coefficient (ADC) mapping. Although many achievements were well represented in such classical maps, another form of representation that could offer complementary information in diffusion data analysis is still needed. In this manner, DC mapping can be helpful. The signal and tissue contrast obtained from the LMC complexity formulation showed an interesting way to analyze other brain tissues poorly represented in classical diffusion analysis.

As shown in Figs. 3 and 4, the DC measurements present a broad range of values that contribute to good tissue segmentation in the diffusion space. All the major brain tissues have a well-delineated order of magnitude for DC signals, maintaining a controlled data variability distribution. Therefore, assuming water self-diffusion behavior in the natural environment, it is clear that brain regions offering low diffusion restriction also have a low complexity level, e.g., CSF. On the other hand, when a rigid diffusion orientation is assumed, mainly on highly dense white matter fibers, the complexity is also penalized, resulting in an intermediate complexity level, e.g., WM. Interestingly, when there is a balance between restrictive environmental conditions and a microstructured self-organized pattern of axons and dendritic connections, the complexity reaches its maximum. This is the case for GM tissue, which provides challenging diffusion modulation using the classical DTI formulation. Hence, it is reasonable to expect the image pattern presented in Fig. 2.

In classical DTI maps, such as FA, it is usually assumed that WM tissue is one of the environments for diffusion modulation due to the dense axonal fibers of the brain. However, many other applications could benefit from diffusion signal analysis in other brain regions, e.g., GM. Therefore, obtaining a novel metric for diffusion images to highlight GM tissue is a positive outcome to be achieved.

Although we have made continued efforts from the scientific community to better understand the DTI-related modality, it is still more appropriate to use the classical DTI imaging protocol, which is more suited to clinical investments and usability. Indeed, advances in new ways to evaluate the diffusion pattern in biological tissue are still a reasonable investment for upcoming advances in medicine, e.g., image reconstruction techniques using Q-ball [31–33], HARDI [34–36], DSI [37–39] and other detailed diffusion modulations and applications [40–43]. However, DTI images can be explored in light of new data analysis procedures, as our proposed method ensures that complementary methods for

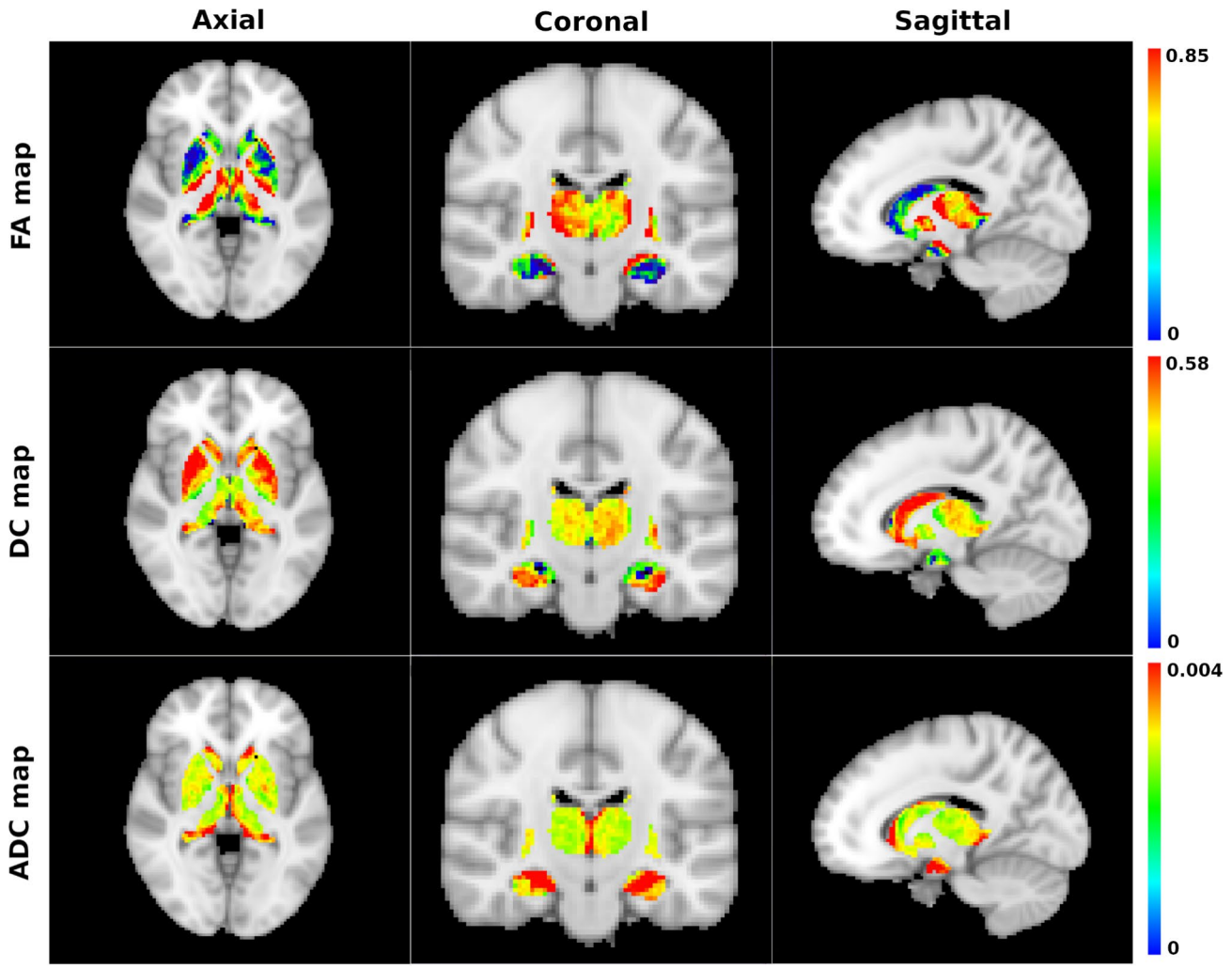

Fig. 5 Subcortical brain regions regarding the FA, DC, and ADC signals (rows). A color-coded representation is provided for each quantitative map to prove the tissue homogeneity throughout the brain region. The DC map presents a consistently greater signal for GM-related cortical and subcortical structures. Furthermore, the values are well spread throughout the spatial structures, representing a smooth but evident differentiation between brain regions. The anatomical labels are given in the supplementary material

obtaining information do not imply an increase in diagnostic cost.

Second, other researchers have reported the properties of entropy calculation for DTI understanding, referring to Shannon's information quantization theory and its application to diffusion space characterization [10–12]. However, our proposed method aggregates the disequilibrium contribution to infer a balance between entirely chaotic behavior and totally restricted previsibility, following the LMC complexity formalism [17]. Hence, it proved to be a good description to infer the intermediate tissue self-organization that is not fully comprehended in the classical DTI schema, especially in the case of the GM tissue.

Another important image pattern highlighted by the DC metric is the ability to identify subtle signal changes in brain regions that are not fully capable of being studied using FA and ADC maps, i.e., subcortical brain regions. As shown in Fig. 5, the general signal distribution through the image space presents a balanced tissue homogeneity and contrast in DC maps, which is not well presented in FA and ADC. Subcortical brain areas were historically challenging for DTI images even though the authors are indicating the importance of evaluating such brain regions [44–47]. There are recent studies that have shown interesting results on DTI measurements in GM-related areas, which foment new investigations on using diffusion data for additional biomarkers on neuroscience and clinical diagnosis. For instance, it has been showing diffusion signal contrast on subcortical areas in primary and secondary progressive Multiple Sclerosis [48], in contrast to the normal-appearance signal in classical MRI maps. Other group studies attest important differences in GM signal on Alcohol dependence [49],

Table 2 Coefficient of variation (CV) for the DC, FA, and ADC maps

Brain area	CV_{DC} ($\mu \pm \sigma$ a.u.)	CV_{FA} ($\mu \pm \sigma$ a.u.)	CV_{ADC} ($\mu \pm \sigma$ mm^2/s)
WM	11,82% ± 6,51%	6,14% ± 4,40%	6,80% ± 1,10%
GM	**8,31% ± 1,03%**	8,60% ± 2,48%	10,08% ± 2,07%
CSF	71,44% ± 14,10%	40,67% ± 16,18%	**17,07% ± 7,65%**
THA	13,09% ± 7,04%	**9,23% ± 4,93%**	19,12% ± 3,69%
CAU	**23,63% ± 14,66%**	25,06% ± 7,45%	35,22% ± 8,39%
PUT	11,51% ± 7,94%	15,91% ± 7,60%	**4,98% ± 0,71%**
PAL	17,94% ± 9,50%	21,93% ± 16,56%	**6,47% ± 0,92%**
HIP	15,82% ± 10,02%	12,48% ± 7,68%	**10,48% ± 2,16%**
AMY	16,01% ± 9,55%	20,81% ± 9,94%	**9,58% ± 1,81%**
ACC	**15,35% ± 7,16%**	26,42% ± 11,82%	19,42% ± 3,21%

The level of signal variation indicates the homogeneity in each brain area. The lower CV value for each row is highlighted. Abbreviations are provided in the supplementary material

chronic neurotrauma [50], association on disturbs of brain-iron concentration [51], and brain cortical delineation [52]. It is worth noticing that the application of diffusion analysis in GM areas has been growing in recent years. Hence, it could be interesting to add new information using new image processing techniques such as the DC map.

In addition, as shown in Fig. 6, there is good signal representation in DC measures for large subcortical structures, e.g., Pallidum and Putamen. In this case, the DC signal variation can be specific to each subcortical region and does not vary abruptly as seen in FA measurements. We presume that the strong signal variation present in FA is more related to the inability to distinguish tissue characteristics due to the tensor representation that is primarily known to struggle with crossing fibers and more complex environments [53–55]. Indeed, the deep gray matter does not present a crossing fibers problem. However, it is a more challenging environment that disturbs tensorial representation. Furthermore, recent findings address the importance of DTI measurements in understanding the brain-iron disturbs and long-term brain structural degeneration [51, 56, 57], adding more insights to the inner complexity of diffusion behavior in biological tissue beyond the crossing fibers issue. This indicates that the DC measure can be more suitable for inferring anatomical changes based on differences in diffusion space distribution that may shift the balance between tissue entropy and disequilibrium considering physical statistical evidence.

Another important consideration in favor of our method is the use of common DWI sequence MRI acquisition, which does not require an additional imaging configuration. In

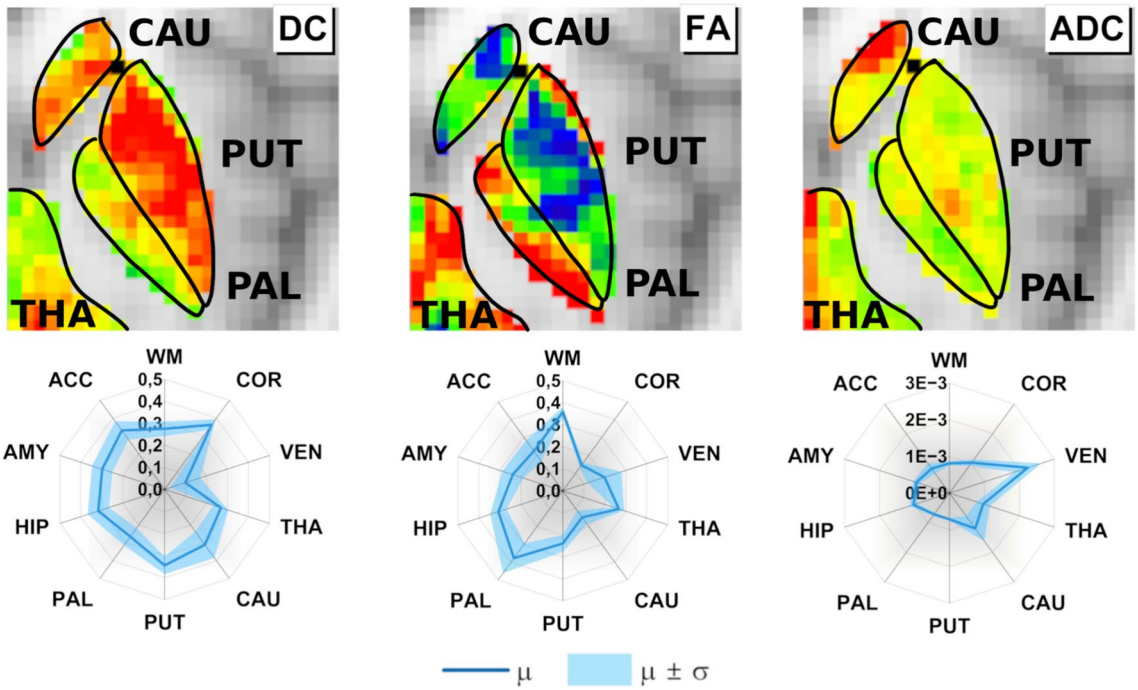

Fig. 6 (First row) Closing representation of the putamen (PUT), caudate (CAU), pallidum (PAL), and partial thalamus (THA); and (second row) signal variability (CV) throughout all the subcortical structures represented in the MNI/Harvard Oxford Brain Atlas, given by DC, FA and ADC maps, respectively. There is evident signal differentiation in cortical and subcortical structures in the DC map, which are not well-delineated in the FA and ADC maps. The same patterns are presented in other subcortical regions. Abbreviations are provided in the supplementary material

this manner, the DC measurement is another good strategy for obtaining novel tissue information by reusing the same image acquisition presented in DTI techniques. There is no need to increase the acquisition cost to obtain the DC map evaluation. This is an advantage, considering the high cost of MRI exams. Therefore, the DC map is entered as complementary information for classical DTI measurements. Another interesting point of view is that the DC algorithm has a low computational cost for DC calculations, which also favors adopting this image processing technique without the need to improve the computational capacity in the clinical or laboratory environment.

Even though interesting points are highlighted for DC measurements, it is also important to discuss its limitations. First, it is known that the adoption of shallow diffusion signal distributions can be problematic for DC estimates. In other words, the quantity of diffusion gradients presented in the DTI imaging acquisition protocol must provide a reasonable amount of diffusion samples per voxel. Hence, DTI images acquired using too few diffusion gradients, e.g., $N < 15$, can result in lower-quality DC maps. In addition, the same can be argued for the assumed b-value for the diffusion orientation (b_1), which should be chosen between $b_1 = 500$ and 2000s/mm^2. Rather than being a specific issue for the DC method, this is general advice for classical DTI formalism, in which it is well-known that the b-value and number of gradients strongly influence classical DTI quantitative maps due to both SNR conditions and tensorial representation. Second, it is also important to consider the partial-volume effect that is particularly relevant in image acquisition with low spatial resolution, such as DTI. In this manner, further quantitative analysis of a small region of interest and a tissue frontier with other anatomical structures, mainly to the CSF interface, is advised. Therefore, although there are interesting findings regarding the brain subcortical areas, as shown in Fig. 6, it should be noted that small subcortical areas must be analyzed with caution.

The DC map generally presents relevant novel information about brain structure organization. The level of understanding in areas that are difficult to study in classical DTI maps, such as GM and subcortical GM, can be greatly improved using DC. This study showed the potential of this new image processing technique, which involves the use of healthy brain anatomical data. However, further analysis must be conducted to better understand the diagnostic potential of DC measurements. It is not within the scope of the present study to analyze cases of brain diseases or brain anatomical changes that occur during natural aging. In special cases, we believe that novel debates will be closely related to the potential of GM discrimination, enabling further analysis in the field of brain diagnosis in presurgical planning for epilepsy, Alzheimer's disease, and Parkinson's disease diagnosis and many other possibilities for the use of DTI images.

Conclusion

The present study proposes a new image processing technique for measuring LMC complexity using the principle of diffusion distribution evaluation on physical statistical formalism. The DC map showed relevant signal characterization in brain tissues and structures historically challenging for classical DTI quantitative mapping, i.e., GM. We believe that the DC technique can be easily applied to many MRI studies requiring the same imaging acquisition for DTI. Our method provides promising complementary information for studying the brain with classical DTI quantitative maps, which can be a rich source of information for further neuroscience research and clinical practice. Further development of DC map use in brain diseases is still needed but shows great potential in light of healthy individual assessments.

Supplementary Information The online version contains supplementary material available at https://doi.org/10.1007/s10334-024-01185-4.

Acknowledgements The authors would like to thank the University of Campinas (Unicamp), São Paulo, Brazil, for their financial support.

Author contributions Material preparation, data collection, analysis and code implementation were performed by Senra Filho, A. C. da S. The first draft of the manuscript was written by Senra Filho, A. C. da S., and all the authors commented on previous versions of the manuscript. All the authors have read and approved the final manuscript.

Declaration

Conflict of interest The authors declare that they have no conflict of interest.

Ethical approval All the authors contributed to the study conception, design and agreement to the journal ethical standards.

References

1. Le Bihan D, Breton E, Lallemand D et al (1986) MR imaging of intravoxel incoherent motions: application to diffusion and perfusion in neurologic disorders. Radiology 161:401–407. https://doi.org/10.1148/radiology.161.2.3763909
2. Drake-Pérez M, Boto J, Fitsiori A et al (2018) Clinical applications of diffusion weighted imaging in neuroradiology. Insights Imag 9:535–547. https://doi.org/10.1007/s13244-018-0624-3
3. Mori S, Zhang J (2006) Principles of diffusion tensor imaging and its applications to basic neuroscience research. Neuron 51:527–539. https://doi.org/10.1016/j.neuron.2006.08.012
4. Viallon M, Cuvinciuc V, Delattre B et al (2015) State-of-the-art MRI techniques in neuroradiology: principles, pitfalls, and clinical applications. Neuroradiology 57:441–467. https://doi.org/10.1007/s00234-015-1500-1

5. Yoshida S, Oishi K, Faria AV, Mori S (2013) Diffusion tensor imaging of normal brain development. Pediatr Radiol 43:15–27. https://doi.org/10.1007/s00247-012-2496-x
6. Meoded A, Poretti A, Mori S, Zhang J (2017) Diffusion Tensor Imaging (DTI)☆. In: Reference Module in Neuroscience and Biobehavioral Psychology. Elsevier
7. Asken BM, DeKosky ST, Clugston JR et al (2018) Diffusion tensor imaging (DTI) findings in adult civilian, military, and sport-related mild traumatic brain injury (mTBI): a systematic critical review. Brain Imag Behav 12:585–612. https://doi.org/10.1007/s11682-017-9708-9
8. Hampton WH, Hanik IM, Olson IR (2019) Substance abuse and white matter: findings, limitations, and future of diffusion tensor imaging research. Drug Alcohol Depend 197:288–298. https://doi.org/10.1016/j.drugalcdep.2019.02.005
9. Lo Buono V, Palmeri R, Corallo F et al (2020) Diffusion tensor imaging of white matter degeneration in early stage of Alzheimer's disease: a review. Int J Neurosci 130:243–250. https://doi.org/10.1080/00207454.2019.1667798
10. Cui J-L, Wen C-Y, Hu Y et al (2011) Orientation entropy analysis of diffusion tensor in healthy and myelopathic spinal cord. Neuroimage 58:1028–1033. https://doi.org/10.1016/j.neuroimage.2011.06.072
11. Delic J, Alhilali LM, Hughes MA et al (2016) White matter injuries in mild traumatic brain injury and posttraumatic migraines: diffusion entropy analysis. Radiology 279:859–866. https://doi.org/10.1148/radiol.2015151388
12. Fozouni N, Chopp M, Nejad-Davarani SP et al (2013) Characterizing brain structures and remodeling after TBI based on information content, diffusion entropy. PLoS ONE 8:e76343. https://doi.org/10.1371/journal.pone.0076343
13. Metwalli NS, LaConte SM, Hu XP (2006) An information theoretic approach characterizing diffusion anisotropy in diffusion-weighted magnetic resonance images. Conf Proc Annu Int Conf IEEE Eng Med Biol Soc IEEE Eng Med Biol Soc Annu Conf 2006:2260–2263. https://doi.org/10.1109/IEMBS.2006.259870
14. Spuhler K, Bartlett E, Ding J et al (2018) Diffusion entropy: a potential neuroimaging biomarker of bipolar disorder in the temporal pole. Synapse 72:e22015. https://doi.org/10.1002/syn.22015
15. Lampinen B, Szczepankiewicz F, Lätt J et al (2023) Probing brain tissue microstructure with MRI: principles, challenges, and the role of multidimensional diffusion-relaxation encoding. Neuroimage 282:120338. https://doi.org/10.1016/j.neuroimage.2023.120338
16. Martinez-Heras E, Grussu F, Prados F et al (2021) Diffusion-weighted imaging: recent advances and applications. Semin Ultrasound CT MRI 42:490–506. https://doi.org/10.1053/j.sult.2021.07.006
17. Lopez-Ruiz R, Mancini H, Calbet X (2010) A statistical measure of complexity
18. Piqueira JRC, de Mattos SHVL (2011) Note on LMC complexity measure. Ecol Model 222:3603–3604. https://doi.org/10.1016/j.ecolmodel.2011.08.012
19. Tournier J-D, Mori S, Leemans A (2011) Diffusion tensor imaging and beyond. Magn Reson Med 65:1532–1556. https://doi.org/10.1002/mrm.22924
20. LaMontagne PJ, Benzinger TL, Morris JC et al (2019) OASIS-3: longitudinal neuroimaging, clinical, and cognitive dataset for normal aging and Alzheimer disease. Medrxiv. 15:2019–2012
21. Poulin P, Theaud G, Rheault F et al (2022) TractoInferno - A large-scale, open-source, multi-site database for machine learning dMRI tractography. Sci Data 9:725. https://doi.org/10.1038/s41597-022-01833-1
22. Roalf DR, Quarmley M, Elliott MA et al (2016) The impact of quality assurance assessment on diffusion tensor imaging outcomes in a large-scale population-based cohort. Neuroimage 125:903–919. https://doi.org/10.1016/j.neuroimage.2015.10.068
23. Lauzon CB, Asman AJ, Esparza ML et al (2013) Simultaneous analysis and quality assurance for diffusion tensor imaging. PLoS ONE 8:e61737. https://doi.org/10.1371/journal.pone.0061737
24. Woolrich MW, Jbabdi S, Patenaude B et al (2009) Bayesian analysis of neuroimaging data in FSL. Neuroimage 45:S173–S186. https://doi.org/10.1016/j.neuroimage.2008.10.055
25. Smith SM, Jenkinson M, Woolrich MW et al (2004) Advances in functional and structural MR image analysis and implementation as FSL. Neuroimage 23:S208–S219. https://doi.org/10.1016/j.neuroimage.2004.07.051
26. Tustison NJ, Avants BB (2013) Explicit B-spline regularization in diffeomorphic image registration. Front Neuroinform 7:39. https://doi.org/10.3389/fninf.2013.00039
27. Avants BB, Tustison NJ, Stauffer M et al (2014) The insight ToolKit image registration framework. Front Neuroinform 8:44. https://doi.org/10.3389/fninf.2014.00044
28. Desikan RS, Ségonne F, Fischl B et al (2006) An automated labeling system for subdividing the human cerebral cortex on MRI scans into gyral based regions of interest. Neuroimage 31:968–980. https://doi.org/10.1016/j.neuroimage.2006.01.021
29. Frazier JA, Chiu S, Breeze JL et al (2005) Structural brain magnetic resonance imaging of limbic and thalamic volumes in pediatric bipolar disorder. Am J Psychiatry 162:1256–1265. https://doi.org/10.1176/appi.ajp.162.7.1256
30. Hua K, Zhang J, Wakana S et al (2008) Tract probability maps in stereotaxic spaces: analyses of white matter anatomy and tract-specific quantification. Neuroimage 39:336–347. https://doi.org/10.1016/j.neuroimage.2007.07.053
31. Caiazzo G, Trojsi F, Cirillo M et al (2016) Q-ball imaging models: comparison between high and low angular resolution diffusion-weighted MRI protocols for investigation of brain white matter integrity. Neuroradiology 58:209–215. https://doi.org/10.1007/s00234-015-1616-3
32. Schilling KG, Nath V, Blaber J, et al (2017) Effects of b-value and number of gradient directions on diffusion MRI measures obtained with Q-ball imaging. In: Medical Imaging 2017: Image Processing. SPIE, pp 179–185
33. Tuch DS (2004) Q-ball imaging. Magn Reson Med 52:1358–1372. https://doi.org/10.1002/mrm.20279
34. Ben Alaya I, Jribi M, Ghorbel F et al (2017) Fast and accurate estimation of the HARDI signal in diffusion mri using a nearest-Neighbor interpolation approach. IRBM 38:156–166. https://doi.org/10.1016/j.irbm.2017.04.003
35. Hutter J, Tournier JD, Price AN et al (2018) Time-efficient and flexible design of optimized multishell HARDI diffusion. Magn Reson Med 79:1276–1292. https://doi.org/10.1002/mrm.26765
36. Vaish A, Rajwade A, Gupta A (2022) TL-HARDI: Transform learning based accelerated reconstruction of HARDI data. Comput Biol Med 143:105212. https://doi.org/10.1016/j.compbiomed.2022.105212
37. Hsu Y-C, Lo Y-C, Chen Y-J et al (2015) NTU-DSI-122: a diffusion spectrum imaging template with high anatomical matching to the ICBM-152 space. Hum Brain Mapp 36:3528–3541. https://doi.org/10.1002/hbm.22860
38. Sun F, Huang Y, Wang J et al (2023) Research progress in diffusion spectrum imaging. Brain Sci 13:1497. https://doi.org/10.3390/brainsci13101497
39. Wang C, Holly LT, Oughourlian T et al (2021) Detection of cerebral reorganization associated with degenerative cervical myelopathy using diffusion spectral imaging (DSI). J Clin Neurosci 86:164–173. https://doi.org/10.1016/j.jocn.2021.01.011
40. Bergamino M, Walsh RR, Stokes AM (2021) Free-water diffusion tensor imaging improves the accuracy and sensitivity of white

matter analysis in Alzheimer's disease. Sci Rep 11:6990. https://doi.org/10.1038/s41598-021-86505-7
41. Bigham B, Zamanpour SA, Zemorshidi F et al (2020) Identification of superficial white matter abnormalities in alzheimer's disease and mild cognitive impairment using diffusion tensor imaging. J Alzheimers Dis Rep 4:49–59. https://doi.org/10.3233/ADR-190149
42. Le H, Zeng W, Zhang H et al (2020) Mean apparent propagator MRI is better than conventional diffusion tensor imaging for the evaluation of Parkinson's disease: a prospective pilot study. Front Aging Neurosci. https://doi.org/10.3389/fnagi.2020.563595
43. McKay JA, Church AL, Rubin N et al (2020) A comparison of methods for high-spatial-resolution diffusion-weighted imaging in breast MRI. Radiology 297:304–312. https://doi.org/10.1148/radiol.2020200221
44. Ganepola T, Nagy Z, Ghosh A et al (2018) Using diffusion MRI to discriminate areas of cortical grey matter. Neuroimage 182:456–468. https://doi.org/10.1016/j.neuroimage.2017.12.046
45. Siehl S, Wicking M, Pohlack S et al (2020) Structural white and gray matter differences in a large sample of patients with Posttraumatic Stress Disorder and a healthy and trauma-exposed control group: Diffusion tensor imaging and region-based morphometry. NeuroImage Clin 28:102424. https://doi.org/10.1016/j.nicl.2020.102424
46. Weston PSJ, Simpson IJA, Ryan NS et al (2015) Diffusion imaging changes in grey matter in Alzheimer's disease: a potential marker of early neurodegeneration. Alzheimers Res Ther 7:47. https://doi.org/10.1186/s13195-015-0132-3
47. Yeh C-H, Jones DK, Liang X et al (2021) Mapping structural connectivity using diffusion MRI: challenges and opportunities. J Magn Reson Imag 53:1666–1682. https://doi.org/10.1002/jmri.27188
48. Woitek R, Leutmezer F, Dal-Bianco A et al (2020) Diffusion tensor imaging of the normal-appearing deep gray matter in primary and secondary progressive multiple sclerosis. Acta Radiol 61:85–92. https://doi.org/10.1177/0284185119852735
49. Kim Y-T, Shim J-H, Kim S, Baek H-M (2021) Diffusion tensor imaging analysis of subcortical gray matter in patients with alcohol dependence. Appl Magn Reson 52:47–60. https://doi.org/10.1007/s00723-020-01272-4
50. Wang L-W, Cho K-H, Chao P-Y et al (2024) White and gray matter integrity evaluated by MRI-DTI can serve as noninvasive and reliable indicators of structural and functional alterations in chronic neurotrauma. Sci Rep 14:7244. https://doi.org/10.1038/s41598-024-57706-7
51. Rulseh AM, Keller J, Tintěra J et al (2013) Chasing shadows: What determines DTI metrics in gray matter regions? An in vitro and in vivo study. J Magn Reson Imag 38:1103–1110. https://doi.org/10.1002/jmri.24065
52. Nagy Z, Alexander DC, Thomas DL et al (2013) Using high angular resolution diffusion imaging data to discriminate cortical regions. PLoS ONE 8:e63842. https://doi.org/10.1371/journal.pone.0063842
53. Reymbaut A, Critchley J, Durighel G et al (2021) Toward non-parametric diffusion- characterization of crossing fibers in the human brain. Magn Reson Med 85:2815–2827. https://doi.org/10.1002/mrm.28604
54. Xue Y, Xie S, Wang X et al (2023) White matter microstructure alterations in idiopathic restless legs syndrome: a study combining crossing fiber-based and tensor-based approaches. Front Neurosci 17:1240929. https://doi.org/10.3389/fnins.2023.1240929
55. Ye Z, Gary SE, Sun P et al (2021) The impact of edema and fiber crossing on diffusion MRI metrics assessed in an ex vivo nerve phantom: Multi-tensor model vs. diffusion orientation distribution function. NMR Biomed 34:e4414. https://doi.org/10.1002/nbm.4414
56. Truong T-K, Guidon A, Song AW (2014) Cortical depth dependence of the diffusion anisotropy in the human cortical gray matter in vivo. PLoS ONE 9:e91424. https://doi.org/10.1371/journal.pone.0091424
57. Tae W-S, Ham B-J, Pyun S-B et al (2018) Current clinical applications of diffusion-tensor imaging in neurological disorders. J Clin Neurol Seoul Korea 14:129–140. https://doi.org/10.3988/jcn.2018.14.2.129